Fusion Engineering and Design 128 (2018) 75–81

Contents lists available at ScienceDirect

Fusion Engineering and Design

journal homepage: www.elsevier.com/locate/fusengdes

Effect of temperature on the corrosion behaviors of 304 stainless steel in static liquid lithium

Xiancai Meng[a,b], Guizhong Zuo[b], Wei Xu[b], Zhen Sun[b], Ming Huang[b], Xiaolin Yuan[b], Chao Xu[c], Wangyu Hu[c], D. Andruczyk[d], Jiansheng Hu[b,e,*], Huiqiu Deng[a,c,**]

[a] Department of Applied Physics, School of Physics and Electronics, Hunan University, Changsha 410082, China
[b] Institute of Plasma Physics, Chinese Academy of Sciences, Hefei 230031, China
[c] College of Materials Science and Engineering, Hunan University, Changsha 410082, China
[d] Center for Plasma Material Interactions, Department of Nuclear, Plasma and Radiological Engineering, University of Illinois Urbana-Champaign, Urbana IL, 61801, USA
[e] CAS Key Laboratory of Photovoltaic and Energy Conservation Materials, Hefei, 230031, China

ARTICLE INFO

Keywords:
Corrosion behaviors
Static liquid lithium
Stainless steel
Temperature
Fusion device

ABSTRACT

The study of the corrosion behaviors of structural materials exposed to liquid lithium (Li) is very important for the application of liquid Li as a potential plasma-facing or blanket material in future fusion device. It was demonstrated that the temperature plays an important role in the corrosion process. The corrosion behaviors of 304 stainless steel (304SS) in static liquid Li at 600 K and 640 K for 1320 h under high vacuum have been compared in the present work. The results show that the weight loss and corrosion depth of the 304SS specimens in static liquid Li at 640 K are about 3 times more than those at 600 K. After exposure to liquid Li, all the surfaces produce non-uniform damage which includes pitting and grain boundary corrosion. The surface damage of 304SS specimens at 640 K is more serious than that at 600 K. The corrosion mechanisms include physical dissolution and chemical corrosion; the effect of the latter on the corrosion behavior at 640 K is much more than that at 600 K.

1. Introduction

Li is a very attractive element in fusion application due to its particular physical and chemical properties, such as low atomic number, low radiating power and strong impurities gettering [1,2]. The melting and boiling temperatures of Li are 454 K and 1616 K, respectively; thus liquid Li has a wide temperature range in liquid state. Liquid Li is not only considered as a potential candidate material for the blanket as a coolant and tritium breeder but also as a plasma-facing components (PFCs) for the inner wall (First Wall) and divertor; therefore, it is being got more attention recently. Blanket concepts using liquid Li are promising for that they can offer a high tritium breeding ratio, high efficiency, low radiation damage for breeders and good thermal transfer [3,4]. Furthermore, in some fusion devices, a dramatic improvement of plasma performance has been observed by using liquid Li surfaces [5–14]. The compatibility of liquid Li with structural materials, especially stainless steels (SSs), is a critical issue because most of the structure materials used are SSs in these systems.

To investigate the compatibility of SSs with liquid Li, a static liquid Li testing device in our group has been built, which can be heated to more than 600 K and pumped to high vacuum. The detailed description of the testing device can be found in our previous paper [15]. The corrosion behaviors of 304SS in static liquid Li at 600 K up to 1548 h were investigated in our previous work [15], where it was found that the weight loss for 304SS specimens increases with the corrosion time and the 304SS specimens suffer from the corrosion by preferential grain boundary attack.

It is known that, aside from the corrosion time, the temperature also plays an important role in the corrosion processes. There are many investigations focused on the compatibility of SSs in liquid Li environments at high temperature (> 773 K). For example, the corrosion behaviors of five different commercial Cr-Mn austenitic SSs (MACR, ICL016, NMF3, Nitronic 32, and Carpenter 18/18 Plus) in static liquid Li at 873 K up to 6000 h were investigated by Ruedl et al. [16], it was observed that all materials showed a penetration of high-angle boundaries by Li. Xu et al. [17,18] found the weight loss of JLF-1 steel at 873 K static liquid Li was larger than that at 773 K, and due to C depletion there was a phase transformation from martensite to ferrite for JLF-1steel at 973 K liquid Li. Li et al. [19] found that the 9Cr-ODS steel exhibited a slight weight loss and decrease in hardness near

* Corresponding author at: Institute of Plasma Physics, Chinese Academy of Sciences, Hefei, 230031, China.
** Corresponding author at: Department of Applied Physics, School of Physics and Electronics, Hunan University, Changsha, 410082, China.
E-mail addresses: hujs@ipp.ac.cn (J. Hu), hqdeng@hnu.edu.cn (H. Deng).

https://doi.org/10.1016/j.fusengdes.2018.01.049
Received 18 September 2017; Received in revised form 18 December 2017; Accepted 21 January 2018
Available online 06 February 2018
0920-3796/

surface and a non-uniform corrosion behavior by preferential grain boundary attack. Its tensile property showed a negligible change and the creep property degraded at 973 K after exposure to liquid Li at 873 K for 250 h.

Despite the numerous experiments regarding the corrosion issues of conventional steels in high temperature liquid Li, the corrosion behaviors or corrosion mechanism of SSs maybe very different at low temperature which is the operational conditions of the liquid Li limiters (LLLs). The experiments of 304SS in static liquid Li at 640 K for 1320 h are carried out and the corrosion behaviors of 304SS in Li at 640 K and 600 K are compared in the present work. The effect of temperature on the corrosion mechanisms of 304SS in LLLs system conditions has been discussed, which is important for further guiding the design and application of components with liquid Li in fusion devices.

2. Experimental conditions

In LLLs systems, the temperature range for liquid Li is between 500 K and 800 K and the vacuum chambers' pressure of fusion devices is less than 10^{-5} Pa [20]. As confirmed by experiments [21,22], the critical wetting temperature range is found to be around 580 K–600 K and the contact angle of liquid Li on SS decreases with an increase of the temperature. When the temperature reaches 640 K, liquid Li has good spread-ability on the surface of SS and the contact angle is about 50°. In 2014, a new flowing liquid Li limiter (FLiLi) with temperature about 640 K based on the concept of a thin flowing film has been successfully tested in the EAST device [14]. Nevertheless, the surface of the FLiLi was damaged by the bombardment of high temperature particles and corrosion of liquid Li. Therefore, the experiments of 304SS in static liquid Li at 640 K for 1320 h under high vacuum (approximately 10^{-5} Pa) are carried out, and the corrosion behaviors of 304SS in Li at 640 K and 600 K are compared in the present work.

3. Experimental setup

The 304SS specimens, Fe-Cr-Ni based austenite SS, are coupon-type ones with the size of 15 mm (Length) × 10 mm (width) × 1 mm (Thickness). The surfaces of the specimens were mechanically polished and cleaned with ultrasound in high purity alcohol before the experiments. Metallic Li was supplied in ingots with high purity of 99.9%, the N content was about 270 ppm. The compositions and ratios of 304SS and Li are listed in Table 1.

The experiments were carried out in a static test facility which has been described in detail previously [15], the experimental procedure was the same as before. The fluctuation range of the temperature was about 5°. Six specimens were dipped into liquid Li (900 g) and the ratio of Li volume V_{Li} (cm^3) to the total surface area S (cm^2) is about 2.14 cm. After being exposing to liquid Li for the expected time, the specimens, which were protected by an Ar atmosphere, were removed from the test vessel when the device cooled to ambient temperature. The remnant Li, covering the specimen surface, quickly lost the metallic luster and became black as a result of reaction with air (forming a complex mixture, Li_3N:Li_2O = 3:1). To avoid the nitride solution, the remnant Li covering the specimens was finally cleaned with high purity alcohol of 99.9%.

The investigations of the specimens were carried out for the weight loss by an electronic balance with an accuracy of 0.01 mg, the morphology and composition by Scanning Electron Microscope (SEM) equipped with an Energy Dispersive X-ray Spectrometer (EDS) and X-ray diffraction (XRD) analysis. For the weight loss, each specimen was measured 5 times and then the average value was obtained.

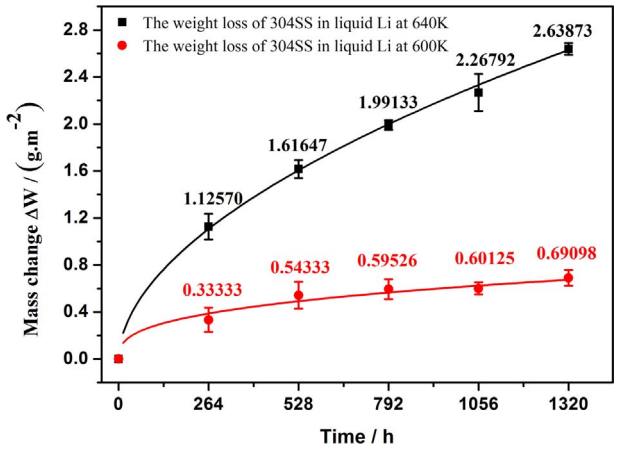

Fig. 1. The weight loss-time curves of 304SS specimens in liquid Li at 600 K and 640 K.

4. The comparison of corrosion behaviors at different temperatures

4.1. Comparison of the weight-loss rate and corrosion depth

The corrosion rate was evaluated by the weight-loss method, where the weight changes for the specimens were obtained before and after exposure to static liquid Li. Fig. 1 shows the weight loss-time curves of 304SS specimens in liquid Li at 600 K and 640 K, respectively. The results show that the weight-loss of 304SS specimens increased slowly with the corrosion time and the weight-loss of 304SS specimens in static liquid Li at 640 K is about 4 times of those in static liquid Li at 600 K. The fitted curves also indicate that the weight loss of 304SS specimens in liquid Li at 600 K and 640 K have an 1/2-power law trend with corrosion time.

4.2. Comparison of the microstructures and compositions

The microstructures and compositions of 304SS specimens before and after being exposed to liquid Li were measured by SEM and XRD, as shown in Figs. 2–4. The 304SS specimen exhibited a metallic luster but many nicks existed on the surface because of the mechanical processing before test, as shown in Fig. 2a. After the remnant Li on the specimens' surfaces was cleaned by water or high purity alcohol, the specimens showed a non-uniform brightness which indicated some inhomogeneous corrosion.

After being exposed into liquid Li at 600 K for 1320 h, the surface of 304SS specimens were slightly damaged. As shown in Fig. 2b, there were a lot of precipitates adhered to the 304SS specimens' surface and the area ratio of precipitates was about 43%. At higher magnification, it was shown that the precipitates were spinel-like with the sizes of 1–2 μm and lots of holes were on the rest of the surface, as shown in Fig. 2c. The EDS and XRD surface analysis showed that the

Table 1
The compositions and ratios of 304SS and Li.

Li	Element	Na	K	Ca	Fe	N	Si	Cl	Al	Ni	Cu
	Content ration%	0.0045	0.0002	0.0015	0.003	0.0027	0.002	0.002	0.001	0.002	0.001
304SS	Composition	Cr	Mo	Mn	Ni	C	Si	Cu	Co	Al	Fe
	Wt%	17.07	2.4	1.0	10.31	0.026	0.34	0.24	0.21	0.045	Bal

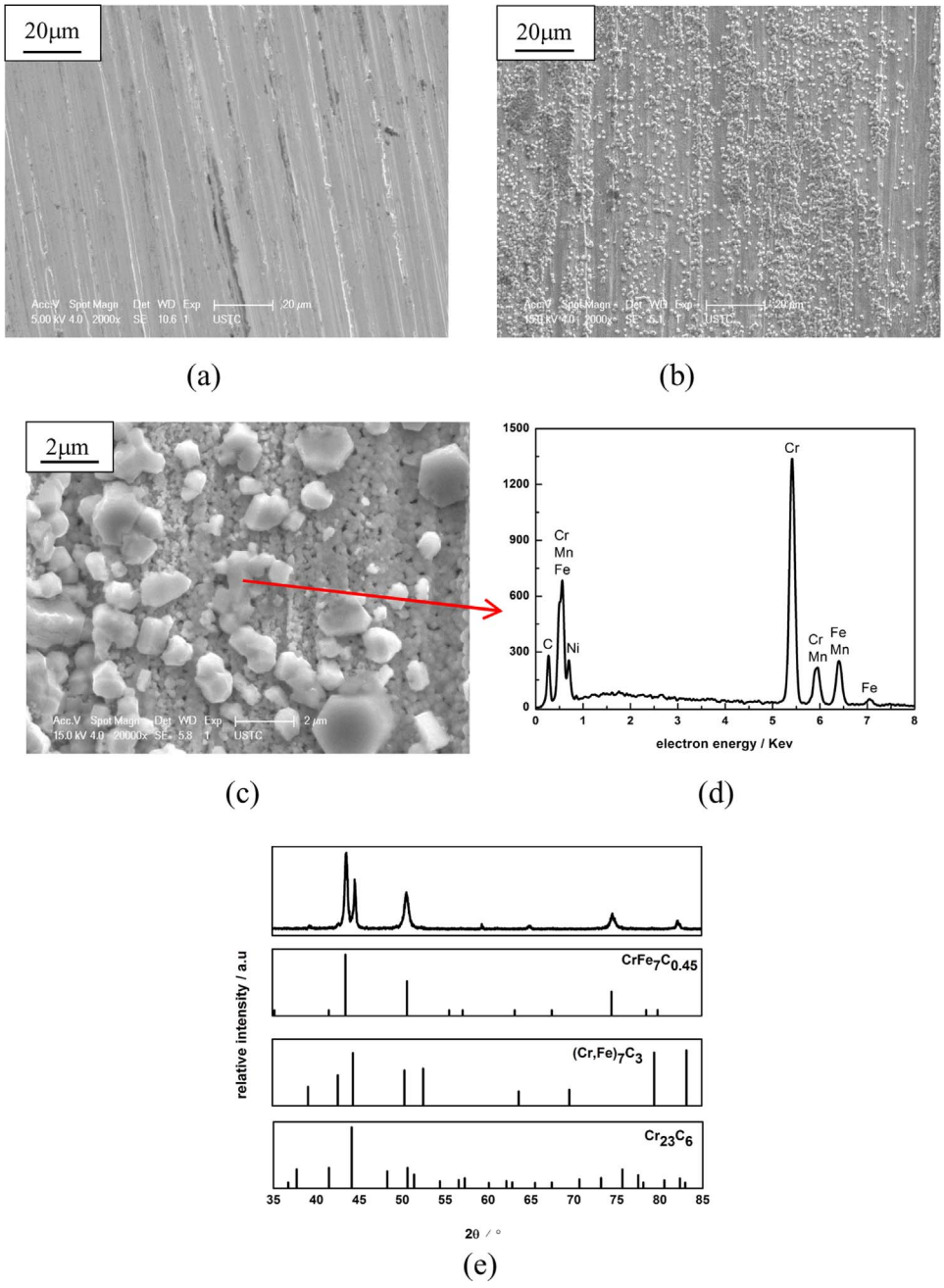

Fig. 2. The microstructures and EDS/XRD surface analysis results of 304SS specimens before and after dipping to liquid Li at 600 K for 1320 h. (a) the initial microstructure of specimen; (b) the microstructure of specimen; (c) the microstructure of corrosion products and holes on specimen [15]; (d) the elements profiles of grains by EDS scanning [15]; (e) XRD analysis result for surface of specimen [15].

compositions of precipitates were mainly Cr and Fe carbides, which included $CrFe_7C_{0.45}$, $(Cr, Fe)_7C_3$ and $Cr_{23}C_6$, as shown in Fig. 2d and e. The details about corrosion behavior of 304SS specimen at 600 K liquid Li were described in our previous study in Ref. [15].

After being dipped into liquid Li at 640 K for 1320 h, the surfaces corrosion of the 304SS specimens were more serious than that at 600 K. As shown in Fig. 3a, there were two types (A and B) of irregular grains adhered to the surface. The irregular grains of type A come in various sizes and agglomerate near the grain boundaries. The number of type B grains was much less than that of type A, but the sizes of the former were much bigger than those of the latter. EDS analyses indicated that the compositions of grains A were mainly Fe and Cr carbides, and those of grain B were Cr nitrides or some complicated compound of nitrides, as shown in Fig. 3b and c. XRD analyses (Fig. 3d) exhibited that the main composition of the corroded surfaces was $CrFe_7C_{0.45}$. In Fig. 4a, some oversized square-like grains with the size about 20 μm were also observed on the surface and they fall off easily duo to the weak adhesion. Fig. 4b showed that there existed an inhomogeneous corrosion, where the initial layer was peeled off and the grain boundaries can be observed clearly. At higher magnification, as Fig. 4c and d shown, the specimens suffered from a typical inter-granular corrosion and pitting attack; the grain boundaries resembled a ravine with 1 μm wide and were attacked to a considerable depth. Cr-depleted zones appeared, where a mass of Cr dissolved from the specimen into liquid Li and/or formed some corrosion products. Lots of holes and parts of irregular but still adherent to the residual layer of corroded surface were observed on the steel bases.

The EDS surface analysis and line scan of the cross-section were performed to determine the composition of the corroded region. After exposure to liquid Li at 640 K and 600 K for 1320 h, the results revealed a slight depletion of Cr and Fe near the surface, as shown in Fig. 5. The thicknesses of corrosion layers were about 5 μm and 2 μm, respectively. Combining the microstructures of the specimens in liquid Li at 640 K, we confirmed that the thickness of corrosion layer should be deeper

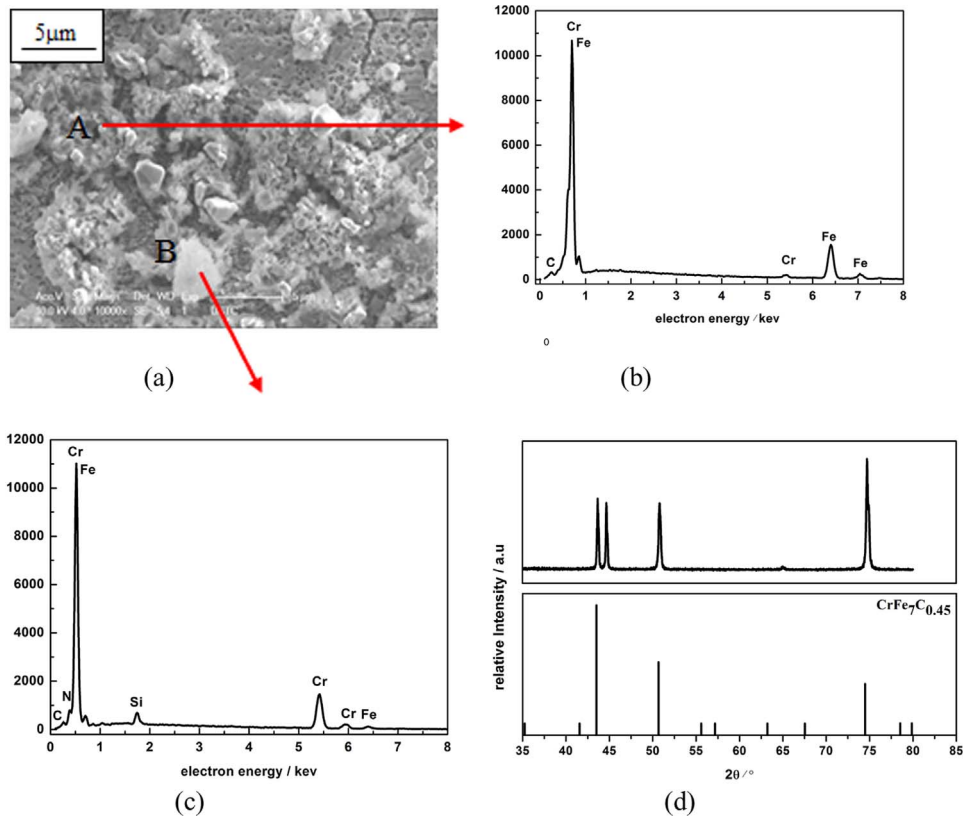

Fig. 3. The microstructures and EDS/XRD surface analysis results of 304SS specimens after dipping to liquid Li at 640 K for 1320 h. (a) the microstructure of specimen; (b) the elements profiles of grains A by EDS scanning; (c) the elements profiles of grains B by EDS scanning. (d) XRD analysis result for surface of specimen.

than 5 μm.

5. Discussion

Based on the obtained results, the corrosion mechanisms of 304SS in liquid Li under the given conditions of experiment include two main aspects: physical dissolution and chemical corrosion. The graph of the corrosion mechanisms is shown in Fig. 6.

For the aspect of physical dissolution, the alloy elements dissolve into liquid metal near the solid-liquid interface. The solubility of the

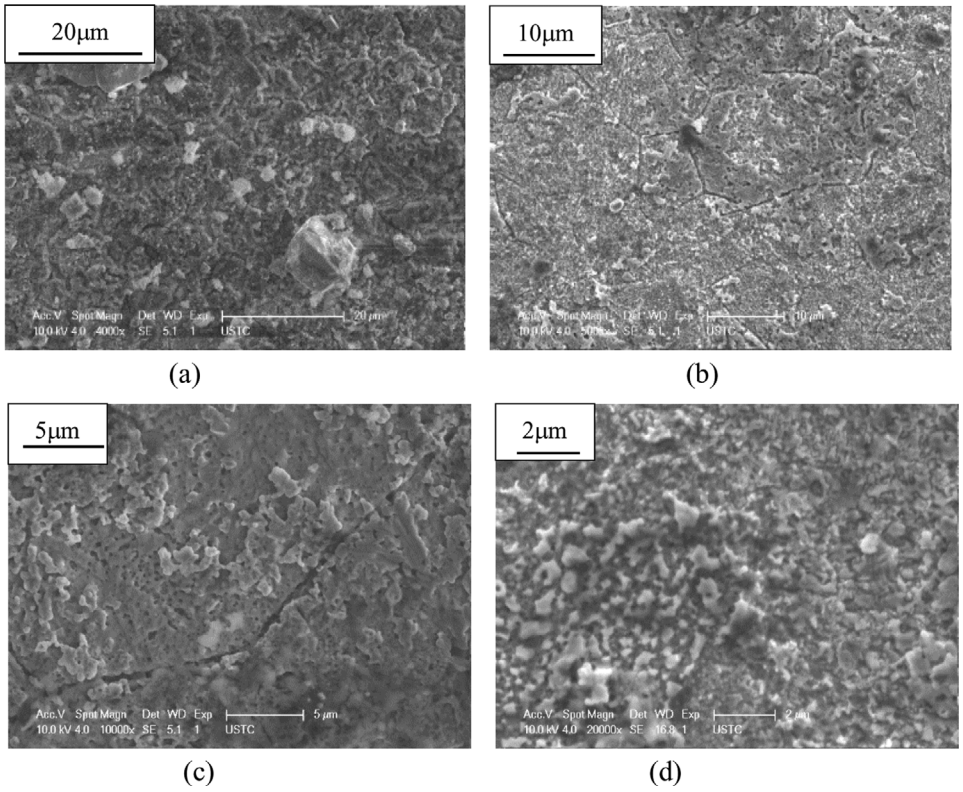

Fig. 4. The microstructures of 304SS specimens after dipping to liquid Li at 640 K for 1320 h. (a) outsize square like grains adhere on the surface; (b) badly damage surface of specimen; (c) grain boundaries were attacked to a considerable depth; (d) residue layer of specimen.

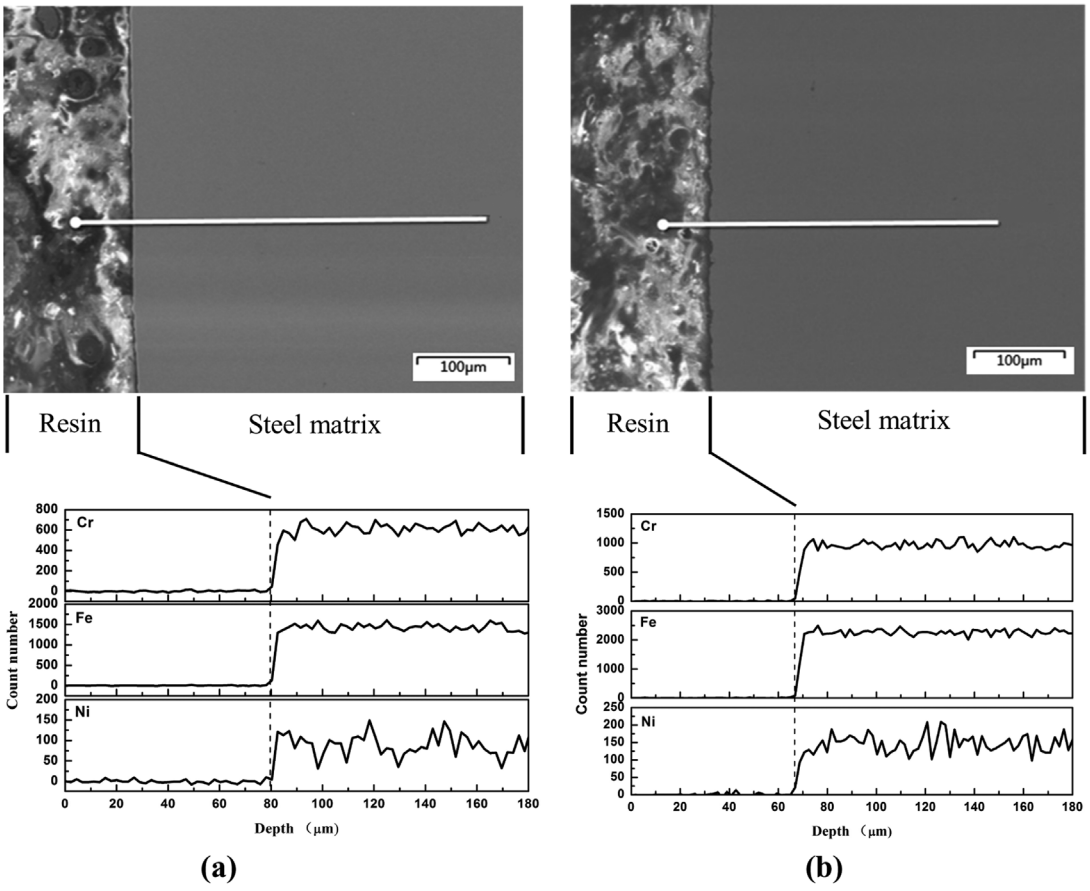

Fig. 5. The thickness of corrosion layers of 304SS after exposure to Liquid Li for 1320 h: (a) at 640 K; (b) at 600 K.

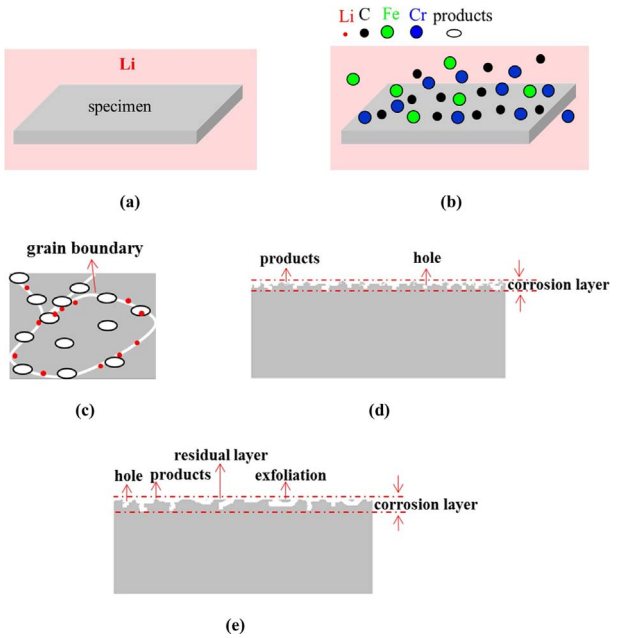

Fig. 6. The graph of corrosion mechanism. (a) initial sate; (b) elements in the alloy dissolve in liquid Li; (c) corrosion products are formed near grain boundaries and Li penetrates to the alloy through the grain boundaries; (d) the cross-section of specimen after exposed to liquid Li at 600 K; (e) the cross-section of specimen after exposed to liquid Li at 640 K.

elements will change with the temperature and the type of liquid metal, thus selective dissolution and corrosion will appear in materials. It's well known that the elements (Cr, Ni, C) in SS can be easily dissolved into liquid Li, as shown in Fig. 6b. For thermally convective Li systems [18,23], some elements are rich or poor in local regions, which result from the mass transfer along the temperature gradient. In high temperature regions, more Ni and Cr are dissolved into liquid Li and the wall of the tube will get thin. Some supersaturated Ni precipitations will generate on the internal surface of the tube in low temperature regions, which could narrow and even block the flow channel. For thermostatic Li systems [3,16,19], the selective corrosion appears because of the preferential selective depletion of alloy elements Cr from SSs in liquid Li.

For the aspect of chemical corrosion, there are two main stages. At the first stage, there occur some intensive chemical reactions among the elements from the specimen and Li near the solid-liquid interface; the products then deposit and grow on the surface of the specimen or in liquid Li, as shown in Fig. 6c. As confirmed in previous work [24,25], the solubility of N and C in liquid Li at 600 K is ~5000 ppm and ~20000 ppm, respectively. The chemical interaction between C and Li can take place easily in liquid state, and C is assumed to be dissolved as Li_2C_2 in liquid Li with low N_2 concentration. As confirmed by corrosion products (Figs. 2e and 3d) and Gibbs-free energy of those products [17,18], the following reactions will occur at the solid-liquid interface

$$14Fe/Cr + 3Li_2C_2 \rightarrow 2Fe_7C_3/Cr_7C_3 + 6Li, \quad (1)$$

$$2Cr + 14Fe + 0.45Li_2C_2 \rightarrow 2CrFe_7C_{0.45} + 0.9Li, \quad (2)$$

$$23Cr + 3Li_2C_2 \rightarrow Cr_{23}C_6 + 6Li. \quad (3)$$

These are the reactions for C depletion from the alloy into liquid Li. Holes will appear near the surface when C dissolves from specimen into liquid Li [18], which result in pitting. Cr is a C-trapper and it can get C atoms from liquid Li easily. The Gibbs free energy of Cr_xC_y is lower than that of Fe_xC_y at the same condition [3], and the diffusion energy of Cr

along the grain boundary (162–252 kJ/mol) is much lower than that in grains (about 540 kJ/mol); therefore, Cr depletes preferentially and Cr carbides prefer to form near grain boundaries.

Furthermore, it's known that the impurity of N can enhance drastically the corrosion aggressiveness of Li [26,27]. Tsisar and Kondo et al. [28,29] claimed that ternary nitrides (Li_9CrN_5) can form on the specimen surface in Li even at low N concentration (around 65wppm) and Li_3FeN_2 can also form if the N potential is sufficiently high. In our experiments, the N concentration in liquid Li is about 270 ppm and the dissolved N is assumed as the form of Li_3N. The following reactions are well known:

$$5Li_3N + Cr \rightarrow Li_9CrN_5 + 6Li, \quad (4)$$

$$2Li_3N + Fe \rightarrow Li_3FeN_2 + 3Li. \quad (5)$$

These products can dissolve in water easily and prefer to be produced at high angle grain boundaries, which promote the dissolution of alloy elements and lead to the penetration of Li into the grain boundaries. In this stage the Cr carbides are formed and the ternary nitride of Li_9CrN_5 are selectively formed; then the Cr concentration in the steel surface is preferentially depleted, and the Cr-depleted zones occur near the grain boundaries.

At the second stage, the liquid Li permeates into surface layer of the specimen through the holes and grain boundaries. The liquid Li can easily permeate into the specimen through the holes which results in C dissolving from the specimen into liquid Li. Li can also penetrates strongly into the grain boundary, as shown in Fig. 6c. At the same time, the formation or presence of carbides near the grain boundaries favors the penetration of Li. It's reported previously that no Li penetration was found at coherent twin boundaries where no carbides were precipitated [23]. Thus, the Li permeates into grain boundaries will be enhanced by the carbides. Also, the penetration of Li into grain boundaries will be induced by ternary nitrides which formed at a boundary. At this stage the surface of the specimen is damaged by large-scale Li attack.

Finally, the dissolution of alloy elements from the specimen is saturated in liquid Li and/or the formation and decomposition rates of corrosion products are equal on the interface. The weight loss tends to constant and the surface damage is also terminated. However, as mentioned in Section 2, an excess of Li (900 g) is used in this experiment and it is difficult for the dissolved elements from the specimen to saturate in a block of Li. Thus, the chemical reactions of formation and decomposition rate of corrosion products play a major role in the equilibrium state.

It is clear that the temperature has a significant effect on the corrosion behavior. 600 K is the critical wetting temperature of liquid Li on SS surface. The elements will dissolve from the specimen into liquid Li and produce some carbides and nitrides at the interface; these compounds will deposit on the specimen surface and produce a layer with the particles of appropriate sizes. Near the interface, the saturated zone composed of the corrosion products and dissolved elements will stop the elements further dissolving from the alloy into the liquid Li and the Li atoms penetrating into the alloy; then the weight loss and surface damage are a dynamic balance. Therefore, there are many particles adhered on the surface and lots of holes on the surface, while it just shows slight surface damage. As mentioned above, Cr depletes preferentially and the Cr carbides and nitrides prefer to produce on the surface, but nitrides could dissolve in water. So the EDS and XRD analysis show that the main compositions of corrosion products are Cr carbides, as show in Fig. 2d and e. Thus, the 304SS in liquid Li at 600 K show a slight weight loss and slight surface damage, as shown in Fig. 6d.

When the temperature of liquid Li is up to 640 K, the solubility of alloy elements (Cr, Ni, and C) in liquid Li is higher than that at 600 K, and the chemical reactions are also enhanced. The corrosion products deposit and grow on the specimen surface, but the particles easily drop out into the liquid Li when their sizes are large enough because of the weak adhesion. Thus, many new grains of various irregular sizes will deposit on the surface. Furthermore, the liquid Li easily permeates into the specimen through the holes and grain boundaries for it has good spread-ability on the surface of SS and a higher kinetic energy when the temperature is higher. The permeated Li like a wedge will expand the width and depth of the holes and cracks, many particles (Cr carbides and nitrides) near the grain boundaries and holes are exfoliated because of their loose binding. In addition, the number of nitrides are much less than carbides, thus EDS and XRD show that the main composition of the corrosion products are Fe carbides, as shown in Fig. 3. As shown in Fig. 6e, when the cracks and/or holes form a closed circuit, the closed-circuit layers drop into the liquid Li from the corroded surface of the specimen. In all the facts studied, if the equilibrium of dissolved products is changed near the surface area, the corrosion will be exacerbated. Thus, the weight of 304SS in liquid Li at 640 K is seriously increased. The surface suffers seriously attack by Li.

6. Conclusion

The effect of temperature on corrosion behaviors of 304SS in static liquid Li was investigated under the operating conditions of LLLs. It's found that the corrosion mechanisms of 304SS in static liquid Li include the physical dissolution and chemical corrosion.

The weight loss of 304SS specimens in static liquid Li at 640 K is about 4 times of that in liquid Li at 600 K. The 304SS specimens show non-uniform corroded morphologies by elemental preferred dissolution, grain boundary corrosion and hole attack. And the surface damage is more serious in liquid Li at higher temperature. The corrosion behavior of 304SS in static liquid Li is sensitive to temperature.

Acknowledgements

The authors would like to acknowledge M. Szott in University of Illinois for fruitful discussion. This research is funded by the National Nature Science Foundation of China under the contract Nos. 11625524, 11405210, 11775261, 11321092, 51371080, 11605246 and the National Magnetic confinement Fusion Science Program. under the contract Nos 2013GB114004, 2013GB114001. This work was also partly supported by the Japan Society for the Promotion of Science-National Research Foundation of Korea-National Science Foundation of China (JSPS-NRF-NSFC) A3 Foresight Program in the field of Plasma Physics (NSFC No. 11261140328). The University of Illinois is supported by the Department of EnergyDE-SC0016322 and Princeton Plasma Physics LaboratoryDE-AC02-09CH11466.

References

[1] J. Sánchez, M. Acedo, A. Alonso, et al., Nucl. Fusion 49 (2009) 104018 {10pp}.
[2] J.S. Hu, Z. Sun, H.Y. Guo, et al., Phys. Rev. Lett. 114 (2015) 055001 {5pp}.
[3] Qi. Xu, Masatoshi Kondo, Takuya Nagasaka, et al., J. Nucl. Mater. 394 (2009) 20–25.
[4] T. Terai, A. Alekseyev, B. Angelini, et al., J. Nucl Mater. 233–237 (1996) 1421–1462.
[5] V. Pericoli-Ridolfini, et al., Nucl. Fusion 47 (2007) S608–S621.
[6] S.V. Mirnov, E.A. Azizov, V.A. Evtikhin, et al., Plasma Phys. Controlled Fusion 48 (2006) 821–837.
[7] K. Ushigusa, M. Seki, K. Suganuma, et al., Fusion Eng. Des. 45 (1999) 137–144.
[8] R. Kaita, R. Majeski, M. Boaz, et al., J. Nucl. Mater. 337 (2005) 872–876.
[9] R. Majeski, S. Jardin, R. Kaita, et al., Nucl. Fusion 45 (2005) 519–523.
[10] G.Z. Zuo, J.S. Hu, J.G. Li, et al., J. Nucl. Mater. 415 (2011) S1062–S1066.
[11] Z. Sun, J.S. Hu, G.Z. Zuo, et al., J. Nucl. Mater. 438 (2013) S899–S904.
[12] J.S. Hu, J. Ren, Z. Sun, et al., Fusion Eng. Des. 89 (2014) 2875–2885.
[13] X.C. Meng, et al., Acta Phys. Sin. 64 (2015) (212801 {10pp}.
[14] J.S. Hu, G.Z. Zuo, J. Ren, et al., Nucl. Fusion 56 (2016) 046011 {14pp}.
[15] X.C. Meng, G.Z. Zuo, J. Ren, et al., J. Nucl. Mater. 480 (2016) 25–31.
[16] E. Ruedl, V. Coen, T. Sasaki, et al., J. Nucl. Mater. 110 (1982) 28–36.
[17] Qi Xu, T. Nagasaka, T. Muroga, et al., Fusion. Sci. Technol. 52 (2007) 609–612.
[18] Qi Xu, Masatoshi Kondo, Takuya Nagasaka, et al., Fusion Eng. Des. 83 (2008) 1477–1783.
[19] Y.F. Li, Hiroaki Abe, Takuya Nagasaka, et al., J. Nucl. Mater. 443 (2013) 200–206.
[20] I.E. Lyublinski, A.V. Vertkov, V.A. Evtikhin, et al., Plasma Devices Oper. 17 (2009)

265–285.
[21] G.Z. Zuo, J.S. Hu, J. Ren, et al., Rev. Sci. Instrum. 85 (2014) 023506 {4pp}.
[22] P. Fiflis, A. Press, W. Xu, et al., Fusion Eng. Des. 89 (2014) 2827–2832.
[23] P.F. Tortorelli, J. Nucl. Mater. 155–157 (1988) 722–727.
[24] K. Natesan, J. Nucl. Mater. 115 (1983) 251–262.
[25] R.J. Pulham, P. Hubberstey, et al., J. Nucl. Mater. 115 (1983) 239–250.
[26] I.E. Lyublinski, V.A. Evtikhin, V. Yu. Pankratov, et al., Nucl. Mater. 224 (1995) 288–292.
[27] R.J. Pulham, P. Hubberstey, et al., J. Nucl. Mater. 115 (1983) 239–250.
[28] V. Tsisar, Masatoshi Kondo, Qi Xu, et al., J. Nucl. Mater. 417 (2011) 1205–1209.
[29] Masatoshi Kondo, Takuya Nagasaka, Takeo Muroga, et al., J. Nucl. Mater. 417 (2011) 1200–1204.